Biosensors and Bioelectronics 194 (2021) 113589

Contents lists available at ScienceDirect

Biosensors and Bioelectronics

journal homepage: www.elsevier.com/locate/bios

Short communication

Molecular profiling of extracellular vesicles via charge-based capture using oxide nanowire microfluidics

Takao Yasui [a,b,c,*], Piyawan Paisrisarn [a], Takeshi Yanagida [d,e,f,**], Yuki Konakade [a], Yuta Nakamura [a], Kazuki Nagashima [b,d], Marina Musa [a], Ivan Adiyasa Thiodorus [a], Hiromi Takahashi [a], Tsuyoshi Naganawa [a], Taisuke Shimada [a], Noritada Kaji [c,g], Takahiro Ochiya [h], Tomoji Kawai [e], Yoshinobu Baba [a,c,i,***]

[a] Department of Biomolecular Engineering, Graduate School of Engineering, Nagoya University, Furo-cho, Chikusa-ku, Nagoya, 464-8603, Japan
[b] Japan Science and Technology Agency (JST), PRESTO, 4-1-8 Honcho, Kawaguchi, Saitama, 332-0012, Japan
[c] Institute of Nano-Life-Systems, Institutes of Innovation for Future Society, Nagoya University, Furo-cho, Chikusa-ku, Nagoya, 464-8603, Japan
[d] Department of Applied Chemistry, Graduate School of Engineering, The University of Tokyo, 7-3-1 Hongo, Bunkyo-ku, Tokyo, 113-8656, Japan
[e] The Institute of Scientific and Industrial Research, Osaka University, 8-1 Mihogaoka-cho, Ibaraki, Osaka, 567-0047, Japan
[f] Institute for Materials Chemistry and Engineering, Kyushu University, 6-1 Kasuga-Koen, Kasuga, Fukuoka, 816-8580, Japan
[g] Department of Chemistry and Biochemistry, Graduate School of Engineering, Kyushu University, Moto-oka 744, Nishi-ku, Fukuoka, 819-0395, Japan
[h] Department of Molecular and Cellular Medicine, Tokyo Medical University, 6-7-1 Nishishinjyuku, Shinjuku-ku, Tokyo, 160-0023, Japan
[i] Institute for Quantum Life Science, National Institutes for Quantum and Radiological Science and Technology, Anagawa 4-9-1, Inage-ku, Chiba, 263-8555, Japan

ARTICLE INFO

Keywords:
Extracellular vesicle
Nanowire
Microfluidics
Extracellular vesicle membrane protein
Nanowire-induced charge-based capture
In-situ profiling of extracellular vesicle membrane protein

ABSTRACT

Extracellular vesicles (EVs) have shown promising features as biomarkers for early cancer diagnoses. The outer layer of cancer cell-derived EVs consists of organotropic metastasis-induced membrane proteins and specifically enriched proteoglycans, and these molecular compositions determine EV surface charge. Although many efforts have been devoted to investigating the correlation between EV subsets obtained through density-, size-, and immunoaffinity-based captures and expressed membrane proteins, understanding the correlation between EV subsets obtained through surface charge-based capture and expressed membrane proteins is lacking. Here, we propose a methodology to profile membrane proteins of EV subsets obtained through surface charge-based capture. Nanowire-induced charge-based capture of EVs and *in-situ* profiling of EV membrane proteins are the two key methodology points. The oxide nanowires allowed EVs to be obtained through surface charge-based capture due to the diverse isoelectric points of the oxides and the large surface-to-volume ratios of the nanowire structures. And, with the ZnO nanowire device, whose use does not require any purification and concentration processes, we demonstrated the correlation between negatively-charged EV subsets and expressed membrane proteins derived from each cell. Furthermore, we determined that a colon cancer related membrane protein was overexpressed on negatively charged surface EVs derived from colon cancer cells.

1. Introduction

Extracellular vesicles (EVs; diameters of 30–2000 nm) are membrane vesicles, such as exosomes, microvesicles, and apoptotic bodies (Evans-Osses et al., 2015; Raposo and Stoorvogel, 2013; Szatanek et al., 2015), and the EVs contain nucleic acids, proteins, and metabolites. The EVs are secreted into the body's blood circulation system by most types of cells. Furthermore, EVs maintain biological functions after their internalization into recipient cells, and therefore, they can regulate cellular information (Bobrie et al., 2011; Schorey and Bhatnagar, 2008; Thery et al.,

* Corresponding author. Department of Biomolecular Engineering, Graduate School of Engineering, Nagoya University, Furo-cho, Chikusa-ku, Nagoya, 464-8603, Japan.
** Corresponding author. Department of Applied Chemistry, Graduate School of Engineering, The University of Tokyo, 7-3-1 Hongo, Bunkyo-ku, Tokyo, 113-8656, Japan.
*** Corresponding author. Department of Biomolecular Engineering, Graduate School of Engineering, Nagoya University, Furo-cho, Chikusa-ku, Nagoya, 464-8603, Japan.
E-mail addresses: yasui@chembio.nagoya-u.ac.jp (T. Yasui), yanagida@g.ecc.u-tokyo.ac.jp (T. Yanagida), babaymtt@chembio.nagoya-u.ac.jp (Y. Baba).

https://doi.org/10.1016/j.bios.2021.113589
Received 30 November 2020; Received in revised form 9 July 2021; Accepted 24 August 2021
Available online 27 August 2021

2009; van Niel et al., 2006; Willms et al., 2016). Since EVs can preserve cancer- and disease-related genetic and proteomic information (Iero et al., 2008; Properzi et al., 2013; Taylor and Gercel-Taylor, 2008), they have been used as a source of cancer and disease biomarkers. To take advantage of their full potential as biomarkers, methodologies that not only capture special subsets of EVs but also profile membrane proteins of EVs are required to identify the correlation between the captured EV subsets and profiled EV membrane proteins. Current methodologies for EV capture are mainly divided into three groups (Szatanek et al., 2015): density-based capture using ultracentrifugation or differential centrifugation (Jeppesen et al., 2019), size-based capture using size exclusion chromatography, and immunoaffinity-based capture (for specific membrane proteins, *e.g.*, CD9, CD63, and CD81). In addition, polymer precipitation (for example, ExoQuick™, a size-based capture according to the kit manufacturer's instruction manual) (Peterson et al., 2015) and microfluidic-based platforms (density-, immunoaffinity-, and size-based captures) (Contreras-Naranjo et al., 2017) have been reported as emerging alternatives. The EV subsets obtained through density-, size-, and immunoaffinity-based captures have EV information corresponding to EV contents or specific membrane proteins (CD9, CD63, or CD81), but not molecular compositions of the EV surface that reflect donor cell information.

Since the outer layer of cancer cell-derived EVs can consist of lipid bilayers, organotropic metastasis-induced membrane proteins (Hoshino et al., 2015), and specifically enriched proteoglycans (Melo et al., 2015), the idea that EVs have a correlation between surface molecules and charge is rational. And therefore, understanding the correlation between EV subsets obtained through surface charge-based capture and expressed membrane proteins should also be important, as is the case with density-, immunoaffinity-, and size-based captures. Fewer efforts have been devoted to investigating the correlation between EV subsets obtained through surface charge-based capture and expressed membrane proteins. Among the developed methodologies, the charge-based capture has advantages of rapid and simple operation with high EV yield and high RNA throughput (Table S1). We previously introduced a nanowire-based concept that could collect over 99% of the EVs present; the analysis targets were urinary microRNAs (Kitano et al., 2021; Yasui et al., 2017). The correlation between EV subsets obtained through surface charge-based capture and expressed membrane proteins has not been addressed as yet, however. Here we propose a methodology using oxide nanowires with different surface potentials to subdivide EVs based on surface charge and we investigate a correlation between surface charge and expressed proteins on the EVs.

2. Materials and methods

2.1. Cell culture and EV purification by ultracentrifugation

Human breast adenocarcinoma cells (MDA-MB-231, American Type Culture Collection Co., Ltd.) were cultured in Dulbecco's modified Eagle's medium (DMEM, Thermo Fisher Scientific Inc.) with 10% exosome-depleted fetal bovine serum (FBS, System Biosciences, LLC.) without any addition of antibiotics. In each passage, 2×10^6 cells were seeded into 15 mL of cell medium in a culturing flask and cultured in an incubator (Panasonic Corp.) at 37 °C and in 5% CO_2. After 48 h, the cell medium was taken from the culturing flask and filtered through a 0.22-μm filter (Merck Millipore Ltd.) to remove cellular debris. Next, 20 mL of the filtered medium was ultracentrifuged (80 min, 4 °C, 110,000g). After discarding the supernatant, we added 10 mL of 0.22-μm filtered phosphate-buffered saline (PBS; Thermo Fisher Scientific Inc.) to wash the collected EVs, and this was ultracentrifuged again (80 min, 4 °C, 110,000g). After discarding the supernatant, 1 mL of 0.22-μm filtered PBS was added to collect EVs, and the collected EVs were stored at 4 °C. For HepG2, HTC116 (American Type Culture Collection Co., Ltd.), CCD-18Co, and Hs578Bst, the media we used were DMEM, McCoy's 5A (American Type Culture Collection Co., Ltd.), Eagle's minimal essential medium (EMEM, American Type Culture Collection Co., Ltd.), and Hybri-Care Medium (American Type Culture Collection Co., Ltd.), respectively. EV zeta potential was measured using commercial apparatuses (Malvern Panalytical Ltd.).

2.2. Nanowire fabrication and characterization

We fabricated ZnO nanowires on Si substrate using the previously reported method (Yasui et al., 2017), and deposited a TiO_2 or a SiO_2 layer on the ZnO nanowires by atomic layer deposition (Figs. S1–S3). The morphology and the composition of ZnO (bare), ZnO/TiO_2 (core/-shell), and ZnO/SiO_2 (core/shell) nanowires were characterized by field emission scanning electron microscopy (FESEM), scanning transmission electron microscopy (STEM) and energy dispersive x-ray spectroscopy (EDS). For the cross-sectional SEM-EDS analysis, we utilized an accelerating voltage of 15 kV. For the single-nanowire STEM-EDS analysis, we used an accelerating voltage of 30 kV. The EDS mapping images were 512 x 384 pixels and the delay time for each pixel was 0.1 ms. The images were integrated for 100 cycles. The peaks of Zn Kα (8.630 keV), O Kα (0.525 keV), Si Kα (1.739 keV), and Ti Kα (4.508 keV) were chosen to construct the elemental mapping images. Nanowire zeta potential was measured using commercial apparatuses (Otsuka Electronics Co., Ltd.).

2.3. EV capture on nanowires

We used a custom-made Teflon holder in the experimental capturing of EVs on each nanowire. The nanowires on a substrate were set into one part of the unassembled holder (Fig. S4a), and the holder parts were then fasted together with screws (Fig. S4b). 1 mL of EV-suspended PBS was supplied to the holder and the EVs were captured onto each nanowire. EV concentration and size were analyzed using a nanoparticle tracking analysis (NTA) instrument (Malvern Panalytical, Ltd.). After appropriate dilutions, video data were collected 5 times for a 60-s time period for each video. Camera level and detection threshold were set to 13 and 5, respectively. Data analysis was performed automatically by NanoSight NTA 3.2 software (Malvern Panalytical, Ltd.). After drying the EVs on the ZnO nanowires, we coated the EVs with gold film using a plasma exposure system (Vacuum Device Inc.) to a thickness around 25 nm for imaging by FESEM (Carl Zeiss AG).

2.4. Nanowire microfluidic device fabrication

A glass substrate (26 × 38 mm, Matsunami Glass Ind., Co., Ltd.) was cleaned and then heated at 300 °C. A solution mixture of 75 mM zinc acetate dihydrate and 75 mM ethanolamine was prepared by dissolving them in 2-methoxyethanol. This solution was used to spin-coat a ZnO layer on the glass substrate (7000 rpm, 30 s), followed by heating of the coated substrate at 300 °C for 3 min; this ZnO layer deposition step was repeated 6 times. Next, positive photoresist (OFPR8600, Tokyo Ohka Kogyo Co., Ltd.) was coated on the substrate (1500 rpm, 120 s) and then the nanowire pattern was formed by photolithography. The ZnO nanowires were grown by immersing the substrate in a solution mixture of 20 mM hexamethylenetetramine (HMTA, Wako Pure Chemical Industries, Ltd.) and 20 mM zinc nitrate hexahydrate (Thermo Fisher Scientific Inc.) at 95 °C for 8 h. After removal of the resist, a sheet of poly (dimethylsiloxane) (PDMS) (Silpot 184, Dow Corning Corp.) patterned with microchannels was bonded to the substrate (Fig. S5).

2.5. In-situ profiling of EV membrane proteins

When introducing EVs into the nanowire device, we allowed the EVs to be captured onto the ZnO nanowires for 1 h at room temperature; then PBS was introduced into the device to remove the uncaptured EVs. Next, we introduced 1% bovine serum albumin (BSA) solution (Kirkegaard & Perry Laboratories, Inc.) into the device and let it stand for 15 min. After washing out the device using PBS, we introduced a mouse monoclonal

anti-human AlexaFluor488-labeled CD63 antibody (10 μg/mL, Santa Cruz Biotechnology, Inc.) or a mouse monoclonal anti-human CD9, CD81, and CD147 antibody (10 μg/mL, Abcam, Plc.) into the device, and let the antibody solution stand for 15 min. Lastly, we washed out the device using PBS. For CD9, CD81, and CD147 detections, additionally, we introduced a goat polyclonal anti-mouse AlexaFluor488-labeled IgG secondary antibody (5 μg/mL, Abcam, Plc.) into the device, and let the secondary antibody solution stand for 15 min. Finally, we washed out the device using PBS and followed that by fluorescence observation with an EM-CCD camera (C9100-13, Hamamatsu Photonics K.K.; measured area, 212 μm^2) through the fluorescence microscope (Olympus, Co., Ltd.), and then the fluorescence intensity was analyzed by image-processing software (AquaCosmos, Hamamatsu Photonics K.K.; measured area, 212 μm^2) (Fig. S6, Supplementary Movie 1).

3. Results and discussion

3.1. Surface charge-based EV capture followed by in-situ profiling of EV membrane protein via the oxide nanowires in microchannels

For charge-based EV capture followed by *in-situ* profiling of EV membrane proteins, we introduce biological samples and then fluorescently labeled antibodies into an array of the oxide nanowires in microchannels; we call this a nanowire device. First, the nanowires harvest EVs from the introduced biological samples, and then, the fluorescently labeled antibodies demonstrate *in-situ* profiling of EV membrane proteins corresponding to the antibody types. Fig. S7 is a schematic of our proposed concept to perform surface charge-based EV capture followed by *in-situ* profiling of EV membrane protein via the nanowire device (Supplementary Movie 1). Oxide nanowires may be a good candidate for EV surface charge-based capture due to the diverse isoelectric points of oxides (Parks, 1965) and the large surface-to-volume ratios of nanowire structures (Rahong et al., 2016; Yasui et al., 2019). The microchannels play an important role in shortening distances and increasing contact frequencies between nanowires and EVs (Sackmann et al., 2014). Since the herringbone structure in our previous design (Kitano et al., 2021; Yasui et al., 2017) generated convection flow, which may have the risk of causing non-charge-based capture of EVs, we fabricated the microchannels without mixing structures (straight channel design). Thus, the present nanowire device allows us to analyze the relationship between surface charge and proteins on EVs.

To confirm the feasibility of charge-based capture on nanowires, we captured EVs onto charged surfaces of the nanowires (Fig. 1a, Supplementary Movie 2). The cell-derived EVs in PBS, which were purified by ultracentrifugation, had a mean zeta potential of −21.0 mV (Fig. 1b) and a mean diameter of about 94.6 nm (Fig. 1c). We deposited two different oxide materials, TiO_2 and SiO_2, on ZnO nanowires to form different surface potentials of the nanowires in the same pH range (Figs. S1–S3). Around pH = 7, the ZnO (bare) nanowires had a positively charged

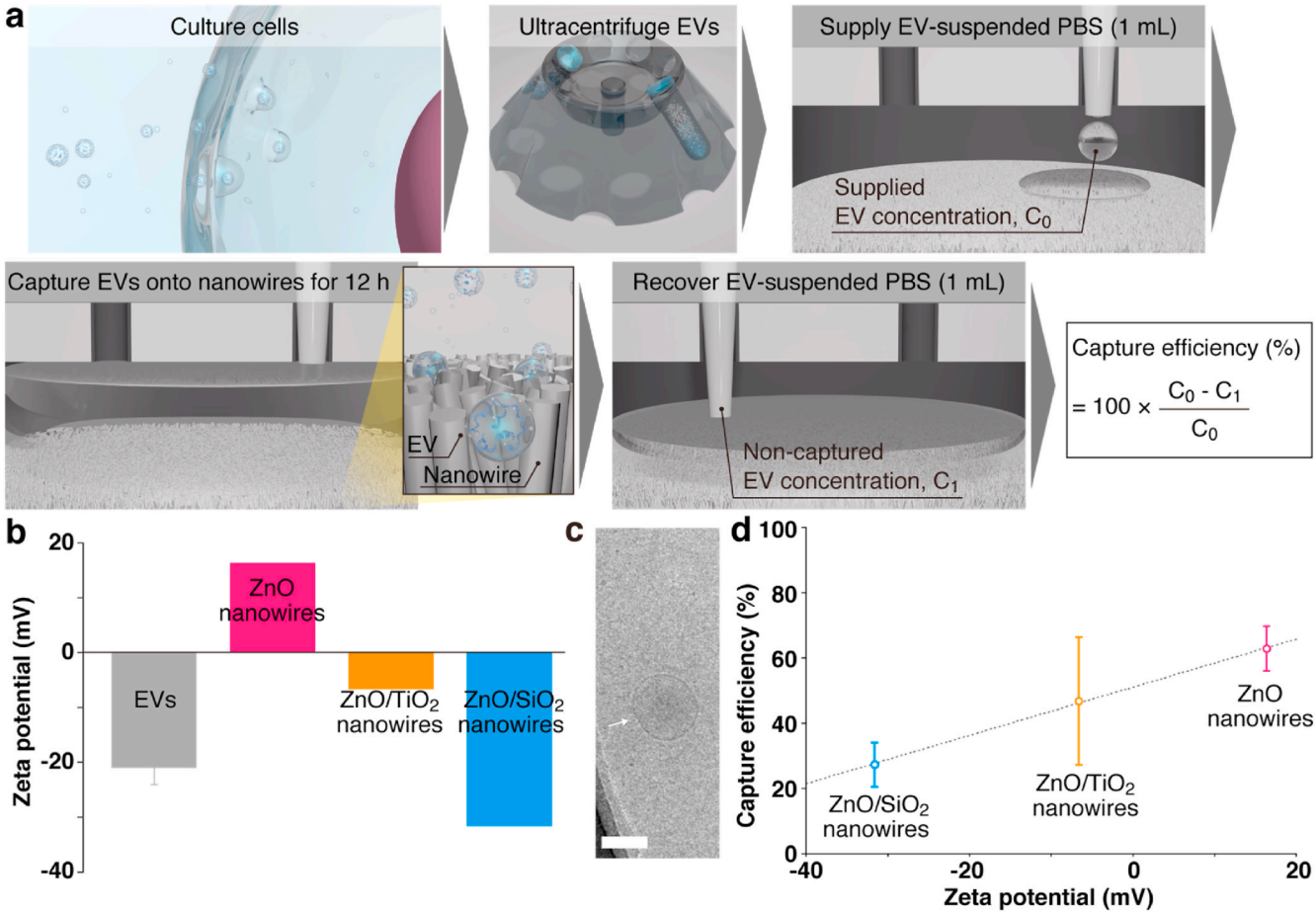

Fig. 1. Nanowire-induced charge-based capture of EVs. (a) Schematic illustrations showing steps in calculating capture efficiency for surface charge-based capture of EVs. (b) Zeta potential of the cell-derived EVs in PBS, and ZnO (bare), ZnO/TiO_2 (core/shell) and ZnO/SiO_2 (core/shell) nanowires in water. (c) A cryo-TEM image of the cell-derived EVs; scale bar, 100 nm. The white arrow indicates the EVs. (d) Capture efficiency of EVs using different material nanowires (pink, ZnO (bare); orange, ZnO/TiO_2 (core/shell); cyan, ZnO/SiO_2 (core/shell)). Nanowires of each material on Si substrate were set into a Teflon holder (Fig. S4) to avoid any unintended adsorption onto the sample holder. Initial concentration of EVs was 1.0×10^9 (/mL). Error bars show the standard deviation for a series of measurements (N = 3). (For interpretation of the references to color in this figure legend, the reader is referred to the Web version of this article.)

surface, and the ZnO/TiO_2 (core/shell) and the ZnO/SiO_2 (core/shell) nanowires had a negatively charged one (Fig. 1b). The ZnO (bare), ZnO/TiO_2 (core/shell), and the ZnO/SiO_2 (core/shell) nanowires could capture EVs in response to the surface potential (Fig. 1d and S4). Although the positively charged surface of the ZnO (bare) nanowires showed the highest capture efficiency among the three types of nanowires, the negatively charged surface of the ZnO/TiO_2 and the ZnO/SiO_2 nanowires could also capture EVs. This result implied that the captured subsets of EVs using each nanowire type were different; the ZnO (bare) nanowires could capture EVs in a charge-based manner, while the ZnO/SiO_2 nanowires could capture EVs in a mechanically entangled manner. The ZnO (bare) nanowires were our first choice in this paper from the standpoint of capture efficiency; however, the ZnO/SiO_2 nanowires also would be good candidates to further investigate EV characteristics of the mechanically entangled EVs. The EV subsets obtained through charge-based capture would provide a unique insight into EV information corresponding to EV contents or specific membrane proteins.

We thought it reasonable that surface potential, density and aspect ratio of nanowires could further improve the capture efficiency of EVs. Considering the relationship between zeta potential of nanowires and capture efficiency, we assumed more positive surface materials, such as NiO, MgO, and PbO (Parks, 1965), would be better suited to enhance the capture efficiency. Since the ZnO surface area relates to the capture efficiency, increasing the nanowire density in the array with enough space for EVs to enter and increasing the aspect ratio of the nanowires by making them thinner and longer, would also offer ways to enhance the capture efficiency. Using a precursor of NiO, MgO, and PbO for atomic layer deposition and adding PEI and ammonia into the growth solution for making nanowires thinner and longer such as done in the literature (Liu et al. 2020a, 2020b; Sakai et al., 2019) would allow researchers to capture more EVs in the nanowire device.

For *in-situ* profiling of the membrane protein of the EVs, here, we used the ZnO (bare) nanowires to capture EVs. We fabricated ZnO nanowires on a glass substrate (Fig. 2a and S5; 700 μm × 15 mm; height, 2 μm) and then bonded a sheet of poly (dimethylsiloxane) (PDMS) with microchannels to the substrate (Fig. 2b; 700 μm × 15 mm; height, 20 μm) to form the nanowire device (Fig. 2c). Analysis of an FESEM image showed that the nanowires had an average diameter of 100 nm and the nanowire density was 20 nanowires/μm^2 (Fig. 2d). We could estimate 2.0×10^8 nanowires were present in the fabricated area, resulting in around a 12-fold larger surface-to-volume ratio compared to the no-nanowire surface. To introduce biological samples, we supplied 1 μL of sample through an inlet, and aspirated the sample using a vacuum pump (Fig. 2e). Considering the spatial volume of one microchannel, we could introduce 0.21 μL amounts of biological samples into the microchannel. Generally, EV concentrations in biological samples (Dragovic et al., 2011) are 10^8-10^{10}/mL and the number of EVs in the microchannel are 2.0×10^5–2.0×10^7. Therefore, we could say that the present nanowire device has a large enough number of nanowires (2.0×10^8 nanowires) to capture EVs, as charge-based subsets, in biological samples.

We verified whether the nanowire device demonstrated *in-situ* profiling of the membrane protein of the charge-based captured EVs onto the ZnO (bare) nanowires. We introduced EVs and fluorescence-labeled antibodies into the nanowire device, and followed that by observing the fluorescence intensities (Fig. S6). Compared with *in-situ* profiling of the membrane protein of EVs in a microchannel without nanowires and no EVs in the nanowire device, we confirmed charge-based EV capture followed by *in-situ* profiling of EV membrane proteins using the ZnO nanowires (Fig. 2f). The FESEM images also allowed us to confirm the EV capture onto the ZnO nanowires (Fig. 2g). To show the superiority of our nanowire-based methodology to the conventional methodology, we used a 96-well plate, protein adsorption platform for comparison (Fig. 2h). Comparison of p-values between the cases of EVs captured onto nanowires and EVs captured onto plate wells of the 96-well plate showed that nanowires could capture EVs and profile membrane proteins efficiently (Fig. 2f and h). We concluded that charge-based EV capture by the nanowire device outperformed protein adsorption-based EV capture by the 96-well plate platform, and our nanowire device was suitable for membrane protein profiling of EVs.

3.2. Correlation between surface charge and membrane proteins

To elucidate a correlation between surface charge and membrane proteins on EVs, we profiled three membrane proteins, CD9, CD63, and CD81, on EVs in the nanowire device. We evaluated the effect of the purification method before introduction into the nanowire device on *in-situ* profiling of the membrane protein of the charge-based captured EVs. Cell-derived EVs in cell medium, without any purification and concentration processes, showed larger fluorescence intensity than those purified and concentrated by ExoQuick and ultracentrifugation (Fig. 2i) with similar CD9/CD81 ratios, though CD63 on EVs using charge-based capture had a little bit higher expression level than for levels obtained using conventional techniques (ExoQuick and ultracentrifugation). The charge-based capture on nanowires could purify and concentrate EVs onto them from cell supernatant. Then, we profiled the expression level of membrane proteins derived from each cell, liver cancer cells (HepG2), breast cancer cells (MDA-MB-231), breast cells (HS578Bst), colon cancer cells (HCT116), and colon cells (CCD-18Co), and determined that each of the cell-derived EVs had unique expression profiles of CD9, CD63, and CD81 (Fig. 2j). As reported using ultracentrifugation, the concentrations of collected EVs differed among different cells and the ratio of expressed membrane protein on EVs also differed among different cells (Borzi et al., 2019; Charoenviriyakul et al., 2017; Dash et al., 2021; Hikita et al., 2018). Reconstruction of the data points of fluorescence intensity clarified that CD9 and CD81 would have an inherent expression level related to each cell type, and CD63 would have an inherent expression level related to EV concentrations (Figs. S8a–S8c). A correlation of expression levels between CD9 and CD81 might be worth considering further; a high expression level of CD9 had a low expression level of CD81 and vice versa. With the ZnO nanowire device, whose use does not require any purification and concentration processes, we demonstrated the correlation between negatively-charged EV subsets obtained through surface charge-based capture and expressed membrane proteins derived from each cell.

Some reports have shown the use of EV membrane proteins in cancer and other disease diagnoses has performance superior to that of standard clinical biomarkers (Im et al., 2014; Logozzi et al., 2009; Yoshioka et al., 2014). Therefore, we profiled CD9 and CD147 membrane proteins, which have both been found to be highly expressed on EVs and on colon cancer related EVs, respectively (Boye et al., 2012; Choi et al., 2012; Edgar, 2016; Evans-Osses et al., 2015; Xiao et al., 2012; Yoshioka et al., 2014). We confirmed that EVs derived from each cell type were captured on the ZnO nanowires and CD9 and CD147 membrane proteins were profiled on the EV surface (Fig. S9), leading to the negatively charged EVs derived from cells being CD9 and CD147 double-positive. Specific membrane proteins on cancer cell-derived EVs seemed to be more highly enriched than those on non-cancer cell-derived EVs (Minciacchi et al., 2015), and the fluorescence intensity of the membrane proteins for cancer cell-derived EVs was higher than that for non-cancer cell-derived EVs even though the EV concentrations were comparable. Profiling membrane proteins of negatively charged EVs demonstrated that colon cancer cell-derived EVs had a significant difference in expression level ratio between CD9 and CD147, compared to other cancer cell-derived EVs and non-cancer cell-derived EVs (Fig. 3a). The breast cancer cell-derived EVs and the breast cell-derived EVs expressed both CD9 and CD147, but there was no significance difference in their expression level ratios (CD147/CD9). Since a correlation between high expression of CD147 and poor prognosis has previously been shown in colorectal cancer (Boye et al., 2012), it makes sense that the present methodology has a potential for *ex-vivo* analysis of tumor-derived EVs.

Finally, we introduced a urine sample from a healthy volunteer into

our microfluidics device and confirmed that EVs in the urine were captured on the ZnO nanowires and CD9 and CD147 membrane proteins were profiled on the EV surface. The present nanowire device satisfactorily profiled membrane proteins of urinary EVs from the healthy volunteer (Fig. 3b). The expression level ratio (CD147/CD9) of urinary EVs from the healthy volunteer showed a significance difference, compared to colon cancer cell-derived EVs and colon cell-derived EVs; however, the expression level ratio (CD147/CD9) of urinary EVs was identical to that of breast cell-derived EVs (Fig. 3c). Considering the fact that the urinary EVs from the healthy volunteer include all EVs derived from all types of cells, it is plausible that the expression level ratio (CD147/CD9) of urinary EVs is identical to that of breast cell-derived

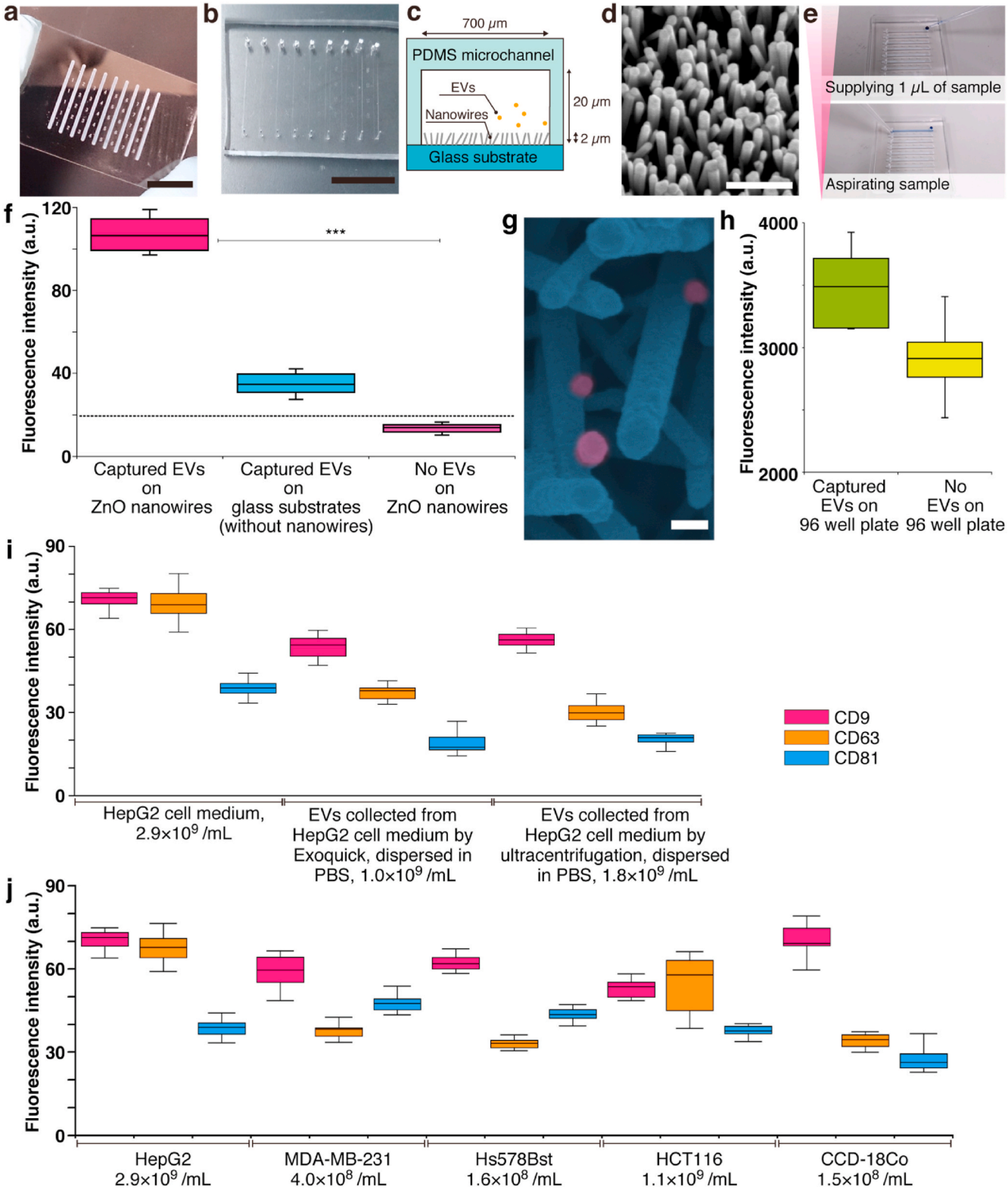

(caption on next page)

Fig. 2. *In-situ* profiling of charge-based captured EV membrane proteins. (a) Photo showing the patterned area of ZnO (bare) nanowires on a glass substrate; scale bar, 10 mm. (b) A photo of a PDMS sheet with fabricated microchannels; scale bar, 10 mm. (c) A schematic cross-sectional illustration of the nanowire device. (d) An FESEM image of ZnO nanowires; scale bar, 1 μm. (e) Photos taken during experimental procedures. (f) Box and whiskers plot of CD63 membrane protein profiling of captured EVs using the microfluidic devices (pink, with ZnO nanowires; cyan, without ZnO nanowires; purple, no EVs). A measurement series was N = 16. Initial concentration of EVs was 1.0×10^{10} (/mL). The horizontal black dotted line shows the signal level at 3 standard deviations above the background (3SD). (g) An FESEM image of captured EVs (colored in pink) on ZnO nanowires (colored in blue); scale bar, 100 nm. (h) Box and whiskers plot of CD63 membrane protein profiling of captured EVs using the 96 well plate (moss green, with EVs; yellow without EVs). A measurement series was N = 6. In (f) and (h), colored box lengths represent the interquartile range (first to third quartiles), the line in the center of each box represents the median value, the bars show the data range (maximum to minimum), and the p-value was calculated by a non-parametric test, the Mann–Whitney *U* test (***p < 0.0001). (i) Box and whiskers plot of membrane protein profiling of captured EVs (pink, CD9; orange, CD63; cyan, CD81). EVs were purified from HepG2 cell-cultured medium by different protocols: no purification, ExoQuick and ultracentrifugation. A measurement series was N = 20. (j) Box and whiskers plot of membrane protein profiling of captured EVs (pink, CD9; orange, CD63; cyan, CD81) in different cell-cultured medium. A measurement series was N = 20. In (i) and (j), colored box lengths represent the interquartile range (first to third quartiles), the line in the center of each box represents the median value, and the bars show the data range (maximum to minimum). (For interpretation of the references to color in this figure legend, the reader is referred to the Web version of this article.)

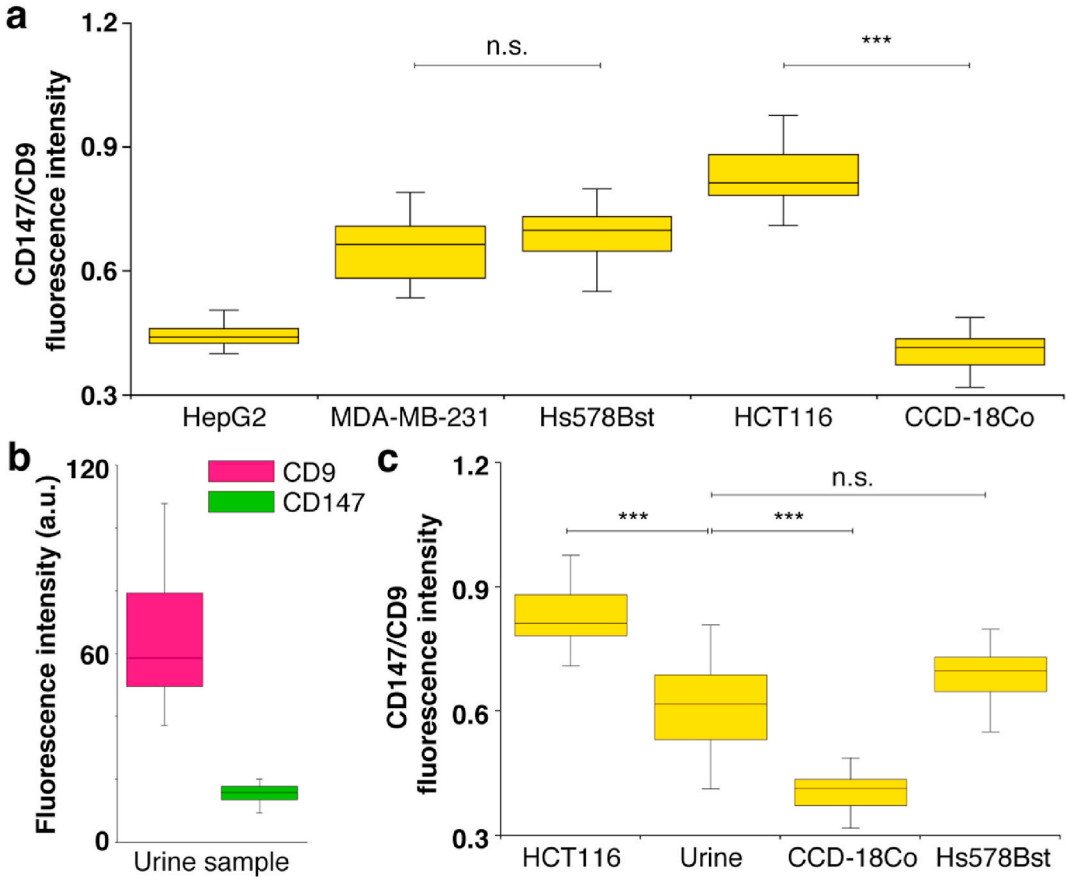

Fig. 3. Membrane protein, CD9 and CD147, profiling of EVs. (a) Box and whiskers plot of the ratio of CD147 fluorescence intensity to CD9 fluorescence intensity. The p-value was calculated by a non-parametric test, the Mann–Whitney *U* test (n.s.: not significant, ***p < 0.0001). (b) Box and whiskers plot of membrane protein profiling of captured EVs (pink, CD9; light green, CD147) in urine. A measurement series was N = 20. (c) Box and whiskers plot of the ratio of CD147 fluorescence intensity to CD9 fluorescence intensity. The p-value was calculated by a non-parametric test, the Mann–Whitney *U* test (n.s.: not significant, ***p < 0.0001). In (a–c), colored box lengths represent the interquartile range (first to third quartiles), the line in the center of each box represents the median value, and the bars show the data range (maximum to minimum). (For interpretation of the references to color in this figure legend, the reader is referred to the Web version of this article.)

EVs and has a significance difference to that of colon cell-derived EVs. These results and previously reported data (Kitano et al., 2021; Yasui et al., 2017) imply that our methodology holds promise for application to urine-based cancer diagnosis.

4. Conclusions

To summarize, we have demonstrated our nanowire device could achieve membrane protein profiling of EV subsets obtained through surface charge-based capture from biological samples. The positively charged surface of the ZnO (bare) nanowires had an important role in the charge-based capture of EVs that we then used for *in-situ* profiling of EV membrane proteins, CD9, CD63, CD81, and CD147. The ZnO (bare) nanowires allowed us to obtain a higher expression level ratio (CD147/CD9) from colon cancer cell-derived EVs and to detect an expression level ratio (CD147/CD9) from the EVs of a healthy volunteer urine sample. Our methodology showed the potential to provide a novel indicator of the EV subset role (surface charge) for cancer diagnosis, although we need to perform further trials for the confirmation of the indicator. Since we have already identified cancer-related microRNAs from urine samples using ZnO nanowires (Kitano et al., 2021; Yasui et al., 2017), we expect it would also be possible to identify the membrane protein-based markers from urine samples after making a correlation between *in-situ* EV profiling and EV-encapsulated microRNAs. At

this point, a startup company (Craif Inc.) has already introduced a ZnO nanowire-based device to the market based on microRNA profiling, and in the future, *in-situ* EV profiling should come to be commercialized widely. Since pH of the solution can affect surface charge of EVs (Midekessa et al., 2020), for future practical use, we need a protocol to adjust this pH by adding pH adjuster solution before supplying sample into the nanowire device. Although we need to perform more trials for cancer diagnosis, the present results have led us to believe our developed approach will be a powerful tool that offers a new strategy for researchers to perform cancer diagnosis using urine samples.

CRediT authorship contribution statement

Takao Yasui: Conceptualization, Methodology, Formal analysis, Investigation, Writing – original draft, Writing – review & editing, Visualization, Supervision, Project administration, Funding acquisition. **Piyawan Paisrisarn:** Methodology, Investigation, Writing – review & editing, Visualization. **Takeshi Yanagida:** Conceptualization, Methodology, Investigation, Supervision, Project administration, Funding acquisition. **Yuki Konakade:** Methodology, Validation, Investigation. **Yuta Nakamura:** Methodology, Investigation. **Kazuki Nagashima:** Methodology, Investigation, Writing – original draft. **Marina Musa:** Methodology, Investigation. **Ivan Adiyasa Thiodorus:** Methodology, Investigation. **Hiromi Takahashi:** Methodology. **Tsuyoshi Naganawa:** Methodology. **Taisuke Shimada:** Methodology. **Noritada Kaji:** Conceptualization. **Takahiro Ochiya:** Conceptualization, Supervision. **Tomoji Kawai:** Conceptualization, Supervision. **Yoshinobu Baba:** Conceptualization, Supervision, Project administration, Funding acquisition.

Declaration of competing interest

The authors declare no competing financial interests.

Acknowledgements

This research was supported by Japan Science and Technology Agency (JST) PRESTO (JPMJPR19H9), JST SICORP (JPMJSC19E3), AMED (Grant Number JP21he2302007 and JP21zf0127004), the JSPS Grant-in-Aid for Scientific Research (S) 18H05243, the JSPS Grant-in-Aid for Scientific Research (B) 21H01960, the JSPS Grant-in-Aid for Exploratory Research 20K21124, the JSPS Grant-in-Aid for Scientific Research on Innovative Areas “Chemistry for Multimolecular Crowding Biosystems”, and research grants from each of the following: the Murata Science Foundation, Advanced Technology Institute Research Grants 2019, Foundation of Public Interest of Tatematsu, the Nitto Foundation, the G-7 Scholarship Foundation, the Nanotechnology Platform Program (Molecule and Material Synthesis) of the Ministry of Education, Culture, Sports, Science and Technology (MEXT), and the Cooperative Research Program of the “Network Joint Research Center for Materials and Devices".

Appendix A. Supplementary data

Supplementary data to this article can be found online at https://doi.org/10.1016/j.bios.2021.113589.

References

Bobrie, A., Colombo, M., Raposo, G., Thery, C., 2011. Traffic 12, 1659–1668.
Borzi, C., Calzolari, L., Ferretti, A.M., Caleca, L., Pastorino, U., Sozzi, G., Fortunato, O., 2019. Cell Death Dis. 10, 759.
Boye, K., Nesland, J.M., Sandstad, B., Haugen, M.H., Mlandsmo, G.M., Flatmark, K., 2012. Br. J. Canc. 107, 667–674.
Charoenviriyakul, C., Takahashi, Y., Morishita, M., Matsumoto, A., Nishikawa, M., Takakura, Y., 2017. Eur. J. Pharmaceut. Sci. 96, 316–322.
Choi, D.S., Choi, D.Y., Hong, B.S., Jang, S.C., Kim, D.K., Lee, J., Kim, Y.K., Kim, K.P., Gho, Y.S., 2012. J. Extracell. Vesicles 1, 18704.
Contreras-Naranjo, J.C., Wu, H.J., Ugaz, V.M., 2017. Lab Chip 17, 3558–3577.
Dash, M., Palaniyandi, K., Ramalingam, S., Sahabudeen, S., Raja, N.S., 2021. Biochim. Biophys. Acta Biomembr. 1863, 183490.
Dragovic, R.A., Gardiner, C., Brooks, A.S., Tannetta, D.S., Ferguson, D.J., Hole, P., Carr, B., Redman, C.W., Harris, A.L., Dobson, P.J., Harrison, P., Sargent, I.L., 2011. Nanomedicine 7, 780–788.
Edgar, J.R., 2016. BMC Biol. 14, 46.
Evans-Osses, I., Reichembach, L.H., Ramirez, M.I., 2015. Parasitol. Res. 114, 3567–3575.
Hikita, T., Miyata, M., Watanabe, R., Oneyama, C., 2018. Sci. Rep. 8, 14035.
Hoshino, A., Costa-Silva, B., Shen, T.L., Rodrigues, G., Hashimoto, A., Mark, M.T., Molina, H., Kohsaka, S., Di Giannatale, A., Ceder, S., Singh, S., Williams, C., Soplop, N., Uryu, K., Pharmer, L., King, T., Bojmar, L., Davies, A.E., Ararso, Y., Zhang, T., Zhang, H., Hernandez, J., Weiss, J.M., Dumont-Cole, V.D., Kramer, K., Wexler, L.H., Narendran, A., Schwartz, G.K., Healey, J.H., Sandstrom, P., Labori, K. J., Kure, E.H., Grandgenett, P.M., Hollingsworth, M.A., de Sousa, M., Kaur, S., Jain, M., Mallya, K., Batra, S.K., Jarnagin, W.R., Brady, M.S., Fodstad, O., Muller, V., Pantel, K., Minn, A.J., Bissell, M.J., Garcia, B.A., Kang, Y., Rajasekhar, V.K., Ghajar, C.M., Matei, I., Peinado, H., Bromberg, J., Lyden, D., 2015. Nature 527, 329–335.
Iero, M., Valenti, R., Huber, V., Filipazzi, P., Parmiani, G., Fais, S., Rivoltini, L., 2008. Cell Death Differ. 15, 80–88.
Im, H., Shao, H.L., Park, Y.I., Peterson, V.M., Castro, C.M., Weissleder, R., Lee, H., 2014. Nat. Biotechnol. 32, 490–495.
Jeppesen, D.K., Fenix, A.M., Franklin, J.L., Higginbotham, J.N., Zhang, Q., Zimmerman, L.J., Liebler, D.C., Ping, J., Liu, Q., Evans, R., Fissell, W.H., Patton, J.G., Rome, L.H., Burnette, D.T., Coffey, R.J., 2019. Cell 177, 428–445.
Kitano, Y., Aoki, K., Ohka, F., Yamazaki, S., Motomura, K., Tanahashi, K., Hirano, M., Naganawa, T., Iida, M., Shiraki, Y., Nishikawa, T., Shimizu, H., Yamaguchi, J., Maeda, S., Suzuki, H., Wakabayashi, T., Baba, Y., Yasui, T., Natsume, A., 2021. ACS Appl. Mater. Interfaces 13, 17316–17329.
Liu, Q.L., Yasui, T., Nagashima, K., Yanagida, T., Hara, M., Horiuchi, M., Zhu, Z.T., Takahashi, H., Shimada, T., Arima, A., Baba, Y., 2020a. J. Phys. Chem. C 124, 20563–20568.
Liu, Q.L., Yasui, T., Nagashima, K., Yanagida, T., Horiuchi, M., Zhu, Z.T., Takahashi, H., Shimada, T., Arima, A., Baba, Y., 2020b. Anal. Sci. 36, 1125–1129.
Logozzi, M., De Milito, A., Lugini, L., Borghi, M., Calabro, L., Spada, M., Perdicchio, M., Marino, M.L., Federici, C., Iessi, E., Brambilla, D., Venturi, G., Lozupone, F., Santinami, M., Huber, V., Maio, M., Rivoltini, L., Fais, S., 2009. PloS One 4, e5219.
Melo, S.A., Luecke, L.B., Kahlert, C., Fernandez, A.F., Gammon, S.T., Kaye, J., LeBleu, V. S., Mittendorf, E.A., Weitz, J., Rahbari, N., Reissfelder, C., Pilarsky, C., Fraga, M.F., Piwnica-Worms, D., Kalluri, R., 2015. Nature 523, 177–182.
Midekessa, G., Godakumara, K., Ord, J., Viil, J., Lättekivi, F., Dissanayake, K., Kopanchuk, S., Rinken, A., Andronowska, A., Bhattacharjee, S., Rinken, T., Fazeli, A., 2020. ACS Omega 5, 16701–16710.
Minciacchi, V.R., Freeman, M.R., Di Vizio, D., 2015. Semin. Cell Dev. Biol. 40, 41–51.
Parks, G.A., 1965. Chem. Rev. 65, 177–198.
Peterson, M.F., Otoc, N., Sethi, J.K., Gupta, A., Antes, T.J., 2015. Methods 87, 31–45.
Properzi, F., Logozzi, M., Fais, S., 2013. Biomarkers Med. 7, 769–778.
Rahong, S., Yasui, T., Kaji, N., Baba, Y., 2016. Lab Chip 16, 1126–1138.
Raposo, G., Stoorvogel, W., 2013. J. Cell Biol. 200, 373–383.
Sackmann, E.K., Fulton, A.L., Beebe, D.J., 2014. Nature 507, 181–189.
Sakai, D., Nagashima, K., Yoshida, H., Kanai, M., He, Y., Zhang, G.Z., Zhao, X.X., Takahashi, T., Yasui, T., Hosomi, T., Uchida, Y., Takeda, S., Baba, Y., Yanagida, T., 2019. Sci. Rep. 9, 14160.
Schorey, J.S., Bhatnagar, S., 2008. Traffic, vol. 9, pp. 871–881.
Szatanek, R., Baran, J., Siedlar, M., Baj-Krzyworzeka, M., 2015. Int. J. Mol. Med. 36, 11–17.
Taylor, D.D., Gercel-Taylor, C., 2008. Gynecol. Oncol. 110, 13–21.
Thery, C., Ostrowski, M., Segura, E., 2009. Nat. Rev. Immunol. 9, 581–593.
van Niel, G., Porto-Carreiro, I., Simoes, S., Raposo, G., 2006. J. Biochem. 140, 13–21.
Willms, E., Johansson, H.J., Mager, I., Lee, Y., Blomberg, K.E.M., Sadik, M., Alaarg, A., Smith, C.I.E., Lehtio, J., Andaloussi, S.E.L., Wood, M.J.A., Vader, P., 2016. Sci. Rep. 6, 22519.
Xiao, D.Y., Ohlendorf, J., Chen, Y.L., Taylor, D.D., Rai, S.N., Waigel, S., Zacharias, W., Hao, H.Y., McMasters, K.M., 2012. PloS One 7, e46874.
Yasui, T., Yanagida, T., Ito, S., Konakade, Y., Takeshita, D., Naganawa, T., Nagashima, K., Shimada, T., Kaji, N., Nakamura, Y., Thiodorus, I.A., He, Y., Rahong, S., Kanai, M., Yukawa, H., Ochiya, T., Kawai, T., Baba, Y., 2017. Sci. Adv. 3, e1701133.
Yasui, T., Yanagida, T., Shimada, T., Otsuka, K., Takeuchi, M., Nagashima, K., Rahong, S., Naito, T., Takeshita, D., Yonese, A., Magofuku, R., Zhu, Z.T., Kaji, N., Kanai, M., Kawai, T., Baba, Y., 2019. ACS Nano 13, 2262–2273.
Yoshioka, Y., Kosaka, N., Konishi, Y., Ohta, H., Okamoto, H., Sonoda, H., Nonaka, R., Yamamoto, H., Ishii, H., Mori, M., Furuta, K., Nakajima, T., Hayashi, H., Sugisaki, H., Higashimoto, H., Kato, T., Takeshita, F., Ochiya, T., 2014. Nat. Commun. 5, 3591.